Design of a Reconfigurable MIMO System for THz Communications Based on Graphene Antennas

Zheng Xu, Xiaodai Dong, *Senior Member, IEEE*, and Jens Bornemann, *Fellow, IEEE*

***Abstract*—Based on the properties of graphene nano-patch antennas, we propose a reconfigurable multiple-input multiple-output (MIMO) antenna system for Terahertz (THz) communications. First, the characteristics of the graphene are analyzed and a beam reconfigurable antenna is designed. The beamwidth and direction can be controlled by the states of each graphene patch in the antenna. Then the path loss and reflection models of the THz channel are discussed. We combine the graphene-based antenna and the THz channel model, and propose a new MIMO antenna design. The radiation directions of the transmit antennas can be programmed dynamically, leading to different channel state matrices. Finally, the path loss and the channel capacity are numerically calculated and compared with those of the Gigahertz (GHz) channel. The results show that for short range communications, the proposed MIMO antenna design can enlarge the channel capacity by both increasing the number of antennas and choosing the best channel state matrices.**

***Index Terms*—Graphene antenna, reconfigurable multiple-input multiple-output (MIMO) system, terahertz (THz).**

I. Introduction

GRAPHENE has attracted much interest since it was first isolated from High Ordered Pyrolytic Graphite (HOPG) in 2004 [1]. Many devices are rebuilt using graphene based on its unique electric properties. For example, for field-effect transistors [2] and interconnects [3], high speed is achieved due to the special energy band structure and ultrahigh electron mobility in graphene [4], [5]. Another promising research topic is graphene-based nano-antennas [6]–[9]. Compared with metallic antennas, the graphene-based nano-patch antennas have a smaller size because of the slow wave property [8], [10], and also resonate with a higher radiation efficiency due to the higher electron mobility in a nano scale structure [9]. Besides, as the resistivity of graphene decreases rapidly with the increase of the electrostatic bias voltage, the states of the graphene-based antennas can be easily controlled. Thus, a reconfigurable antenna array with variable radiation patterns is obtained based on this characteristic [6], [11].

On the other hand, the multiple-input multiple-output (MIMO) antenna technique is well known to increase the spectral efficiency of a wireless communications system [12]. If the amount of scattering and reflections in the multi-path environment is large enough, then more transmit and receive antennas result in more data streams and higher spectral efficiency. However, for real MIMO systems with limited area, the antenna size and antenna separation are the main obstacles to increasing the MIMO scale, which is difficult to solve when using traditional omnidirectional antennas. To deal with this problem, graphene-based directional antennas can be promising candidates to decrease the antenna size [8]. Also, high directional antennas can reduce the antenna separation by enlarging the angular spread. Another way to increase spectral efficiency is using reconfigurable antennas. For example, by controlling the antenna length [13], [14] or the states of the antenna array [6], [11], the radiation pattern is changed dynamically, which increases the spectral efficiency by 10%–70%.

In the long term, the only promising way to meet the demand of ultra high data rate is to shift the carrier frequencies to the Terahertz (THz) band. However, the THz channel has many characteristics different from the Gigahertz (GHz) channel, such as much higher propagation loss and extra molecular absorption loss [15]. Thus, the models for the GHz channel cannot be applied directly to the THz channel. Reference [15] models the THz channel and analyzes the capacity of wireless networks. The results show that the capacity can be as high as 100 Tbit/s but drops quickly because the path loss for long distance is relatively high. To conquer this problem, the authors in [16] suggest to use highly directional antennas at THz frequencies in realistic indoor environments. Besides the path loss, the scattering and reflection behaviors are also different from those in the GHz band[17], [18]. For THz waves, the surfaces of indoor objects must be regarded as rough surfaces instead of smooth surfaces. When the surface is rough enough, the specular reflection may lose its privileged position, and the diffusely scattered paths may be even stronger[19]. Therefore, these unique features lead to new models to characterize the THz channel.

For THz communications, new antenna designs are needed to adapt to the THz channel. Reference [20] studies the THz emission from interdigitated finger photomixers coupled to planar antenna structures, and reveals that the performance can be improved by independently optimizing the photomixer and antenna. Georgiou *et al.* have recently demonstrated experimentally a full all-optical generation of linear antennas at THz frequencies, indicating the possibility of inducing resonant phenomena by the structured illumination of a flat surface [21]. However, both of these antennas are not suitable for building reconfigurable directional antennas. Besides, for nano-devices, such as nano-sensors and nano-on-chip systems [22], [23], the space is limited and the sizes of the aforementioned antennas are too large (i.e., the size of the antenna in [21] is about several

Manuscript received April 01, 2014; revised May 18, 2014; accepted June 03, 2014. Date of publication June 30, 2014; date of current version August 22, 2014. *(Corresponding author: Zheng Xu.)*

The authors are with the Department of Electrical and Computer Engineering, University of Victoria, Victoria, BC V8W 3P6, Canada (e-mail: zhengxu@ece.uvic.ca; xdong@ece.uvic.ca; jbornema@ece.uvic.ca).

Digital Object Identifier 10.1109/TTHZ.2014.2331496

millimeters). As graphene has the aforementioned novel properties, it can satisfy our requirements in manufacturing reconfigurable directional antennas for THz communications. References [24] and [25] combine leaky-wave theory and the properties of graphene, and propose two different antenna structures with beam scanning capabilities. However, in order to tune the radiation patterns, many different bias voltages (as high as 45 V) are required [25] which is complicated for a nano device. Besides, for both of these two designs, the gains of the antennas are small and cannot compensate the high path loss in the THz.

In this paper, a new reconfigurable MIMO antenna system for THz communications is designed based on graphene Yagi–Uda antennas. The main contributions of this work are summarized as follows.

- We propose a Yagi–Uda antenna design based on an array of graphene patches for the first time, and analyze the radiation patterns of these directional antennas, which can be easily configured by changing the electrostatic bias voltage on each element.
- Based on the THz channel model, we propose a new MIMO antenna system for THz communications. The transmitter in the system is an array of antennas and each antenna is an array of graphene patches.
- We firstly apply the designed reconfigurable graphene-based directional antennas to THz MIMO systems, and analyze the spectral efficiency of such MIMO systems under different scenarios. We show for the first time that the antenna separation can be tremendously reduced if directional antennas are used.
- We investigate the performance of such a reconfigurable MIMO system via simulations. The results are compared between different power allocation schemes as well as with the performance of traditional metallic antenna based MIMO systems. It is shown that by employing the best configuration, our system can considerably increase the spectral efficiency.

The remainder of this paper is organized as follows. In Section II, we provide the background information of graphene and graphene-based antennas. In Section III, we model the THz channel and compare it with the GHz channel. Then, a new graphene-based MIMO antenna system is proposed in Section IV. The spectral efficiency of such system as well as the simulation results are discussed in Section V. Finally, our conclusions are given in Section VI.

II. Graphene-Based Directional Antennas

Graphene is a two-dimensional, infinitesimally thin sheet with a surface conductivity $\sigma(\omega, \mu_c, \Gamma, T)$, where ω is the radian frequency, μ_c is the chemical potential, Γ is the phenomenological scattering rate, and T is the temperature. Spatial dispersion effect may become significant under certain conditions, which modifies the characteristics of graphene-based devices [26]. When the spectral wave number is extremely large, the full-k_ρ relaxation time approximation model is introduced to characterize the conductivity of graphene [27]. In this work, the normalized wave number (normalized with respect to the free space wave number) is between 50–100, and hence the spatial dispersion effect can be ignored [27]. Therefore, we can use the results from the Kubo formula [28]

$$\begin{aligned}&\sigma(\omega, \mu_c, \Gamma, T)\\ &= \frac{je^2(\omega - j2\Gamma)}{\pi\hbar^2}\left[\frac{1}{(\omega - j2\Gamma)^2}\int_0^\infty \varepsilon\left(\frac{\partial f_d(\varepsilon)}{\partial\varepsilon} - \frac{\partial f_d(-\varepsilon)}{\partial\varepsilon}\right)d\varepsilon\right.\\ &\quad \left. - \int_0^\infty \left(\frac{f_d(-\varepsilon) - f_d(\varepsilon)}{(\omega - j2\Gamma)^2 - 4\left(\frac{\varepsilon}{\hbar}\right)^2}d\varepsilon\right]\right. \qquad (1)\end{aligned}$$

where $-e$ is the charge of an electron, $\hbar$ and h are the reduced and normal Planck's constants, k_B is the Boltzmann's constant, and $f_d(\varepsilon) = (e^{(\varepsilon-\mu_c)/k_BT} + 1)^{-1}$ is the Fermi–Dirac distribution. The relationship between μ_c and the carrier density n_s is [29]

$$n_s = \frac{2}{\pi\hbar^2 v_F^2}\int_0^\infty \varepsilon[(f_d(\varepsilon) - f_d(\varepsilon + 2\mu_c)]d\varepsilon, \qquad (2)$$

where v_F is the Fermi velocity. Therefore, the chemical potential μ_c is determined by the carrier density which can be controlled by application of a electrostatic bias voltage and chemical doping [29]. For a single layer graphene (SLG), suppose the bias voltage is V_g. Then, for each density of charged impurities n_{imp}, there exists a corresponding bias voltage $V_g = V_D$ that makes the conductivity of the graphene maximum. When $V_g = 0$, the conductivity of the graphene is minimized. In this work, the bias voltage $V_D = 15$ V [6]. If n_{imp} is large enough, the maximum conductivity of the highly doped graphene can be 10 000 times larger than the minimum conductivity [6], [29]. Therefore, graphene has two modes: the low resistance mode when $V_g = V_D$, and the high resistance mode when $V_g = 0$.

Graphene-based nano-patch antennas for THz communications usually have a dimension on the order of microns. As the width of the patches is finite, the edges of the graphene may modify the guiding properties of plasmons [24], [30]. In the THz range, there are two types of plasmon modes within the graphene patches: the waveguide mode and the edge mode. For the low frequency in our work ($<$ 2 THz), there is only one mode [30]. Besides, in this work, the width of the graphene patches is fixed and, therefore, the plasmon-light coupling angle is constant. We can directly synthesize different graphene patterns using chemical vapor deposition on thin nickel layers and transfer them to arbitrary substrates [31]. Although current technologies cannot fabricate graphene antennas with high efficiency, they might still be used in applications where low efficiency is tolerated and small antenna size is required. A nano-patch antenna sample made of graphene on SiO_2/Si substrate is shown in Fig. 1(a). In this example, the dimensions of the antenna are 2 μm $\times$ 5 μm which resonates at 1 THz [9]. This resonant frequency is much lower than that of the standard metallic dipole antennas of the same size. A photomixer is employed to couple the wave into graphene antennas, as explained in details in [32]. As an alternative, the wave can also be coupled by means of electric pumping [33], [34]. A electrostatic bias voltage is applied on the graphene to change its resistance modes. Suppose 1 THz is the resonant frequency at the low resistance mode. When the graphene changes to high resistance mode, the resonant frequency shifts away from 1 THz. For the fixed feeding frequency of 1 THz, the graphene

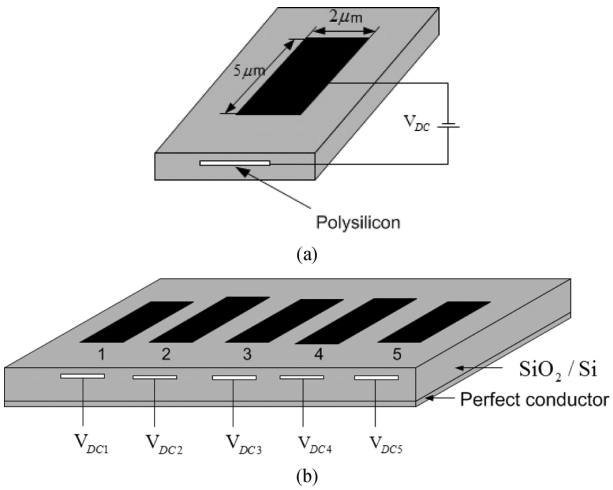

Fig. 1. (a) Graphene-based nano-patch antenna element. (b) Graphene-based directional antenna with 5 elements, and each element has a similar size as the one in (a).

patch resonates when $V_g = V_D$, and does not resonate when $V_g = 0$. Therefore, by changing the bias voltage, the radiation states can be configured dynamically.

Recently, in order to adapt to the changing channels, reconfigurable antennas attract much interest in wireless communications [14]. In some scenarios, the length of the antenna can be dynamically changed so that the resonant frequency can vary. In some other cases, the reconfiguration features can be obtained by using phased antenna element arrays. Based on the aforementioned properties, we further consider a Yagi–Uda-based reconfigurable antenna with m patch elements, as shown in Fig. 1(b). The patch in the middle is used as the driven element, the two nearby patches $(2, 4)$ are used as reflectors and all others are used as directors. The lengths of the reflectors are 7% longer than the driven element and the directors are 14% shorter than the driven element. There is a reflection sheet $\lambda/4$ below the antenna elements. Let c_i denote the mode of the ith graphene patch element and the mode set $[\mathbf{C}]_i = c_i$, where $\mathbf{C}$ is a vector. The commercial software HFSS is used to simulate the radiation patterns of the antenna. By keeping some graphene patches in the low resistance mode while others in the high resistance mode, different radiation patterns are produced. For example, when patches 1, 3, 4 are in the low resistance mode and 2, 5 are in the high resistance mode, the radiation pattern is shown in Fig. 2(a). In this case, the driven element (the 3rd patch) is excited by a 1 THz wave, and the reflector (the 4th patch) and the director (the 1st patch) are passive radiators and do not need feeding. At this stage, the significance of the coupling effects between two nearby graphene patches is not clear, and needs to be explored in future work. In this paper, such coupling effects are assumed negligible. Fig. 2(b)–(c) shows the radiation directions with other configurations which have a size of 5. Fig. 2(a) and (b) indicates that the radiation direction has a dynamic range up to 80° and the beamwidth is 50°. Also, the beamwidth of the antenna can be modified by changing the number of elements. Fig. 2(d) shows the beamwidth of an antenna with seven elements. In this case, the patches 1, 4, 7 are in the low resistance mode and 2, 3, 5, 6 are in the high resistance

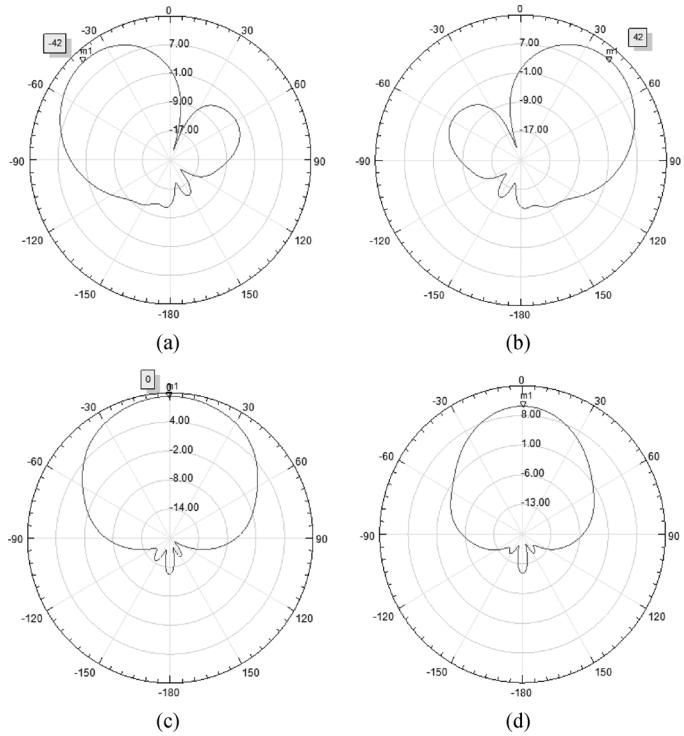

Fig. 2. Radiation pattern of the antenna for $\mu_c = 1$ eV, $\Gamma = 1 \times 10^{12}$, $T = 300$ K, and the size of the driven element is 2 μm×5 μm. The number of elements in (a)–(c) is 5; and (d) 7. (a) Elements 1, 3, and 4 are in the low resistance state. (b) Elements 2, 3, and 5 are in the low resistance state. (c) Elements 1, 3 and 5 are in the low resistance state. (d) Elements 1, 4, and 7 are in the low resistance state. The working frequency $f = 1$ THz.

mode. Patch 4 acts as the driven element, and patches 1, 7 are the reflector and the director, respectively. Similar to Fig. 2(c), the radiation direction is 0°, as the reflector and the director have the same length. Obviously, the beamwidth is narrower and the gain is higher than those of 5 elements. Fig. 2 indicates that we can get highly directional antennas with a narrow beamwidth by properly choosing the number of elements and the states of each element. Moreover, compared with the structure in [35], patches in high resistance mode do not introduce any interference to the desired patterns. Therefore, the graphene-based antenna has some distinctive properties suitable for THz communications systems. First of all, the size of antennas made of graphene is smaller which is important for devices in the THz band. Secondly, the radiation direction can be conveniently configured by changing the electrostatic bias voltage. Finally, the antenna is highly directional and with a high gain so that it can compensate for the high attenuation loss in the THz band.

III. Model of THz Channel

In order to increase the spectral efficiency to meet the requirements of future wireless communications in current frequency bands, advanced modulation schemes and signal processing technologies are not enough. Therefore, the THz band (0.1–10 THz) is regarded as one of the most promising spectrum bands. The THz channel model has been discussed in several recent works [15], [17], [18], [36], [37], and in this paper, we use the results in [15]. A signal in the THz band suffers both spreading loss and molecular absorption loss, which is different

from that in the GHz band in which molecular absorption loss can be ignored. The total path loss in the THz band is [15]

$$A(f,d) = A_{\text{spread}}(f,d) + A_{abs}(f,d), \tag{3}$$

where $A_{\text{spread}}(f,d)$ is the spreading loss at distance d and frequency f, defined in decibels (dB) as

$$A_{\text{spread}}(f,d) = 20\log\left(\frac{4\pi f d}{c}\right) \tag{4}$$

where c is the speed of light in free space, and $A_{abs}(f,d)$ is the molecular absorption attenuation denoted in dB as

$$A_{abs} = k(f)d10\log_{10} e, \tag{5}$$

where $k(f)$ is the medium absorption coefficient. As the air is the composition of different molecules (e.g., nitrogen, oxygen and water vapor), $k(f)$ is the sum of weighted coefficients of each gas. When the concentration of the water vapor is high, several peaks of attenuation are observed due to the molecular absorption loss, and the total band is segmented into several transmission windows. Except for these peaks, the total path loss only depends on the distance and the frequency, independent of the molecular composition, which is similar to that in the GHz band. Equation (4) indicates that the spreading loss in the THz band is 60 dB higher than that in the GHz band, thus the THz frequency is only suitable for short range communications.

Besides the differences in path loss, the reflection properties are also different from those in the GHz band. For objects (e.g., plaster or wallpaper) in indoor environments, the surface variations are on the order of several hundred microns to millimeters [17], [18], which are comparable to the THz wavelength λ (e.g., wavelength at 1 THz is 300 microns). Therefore, the surfaces of indoor objects, which can be regarded as smooth surfaces at the GHz frequency, are now rough surfaces at the THz frequency. According to the analysis in [19, p.81], the roughness factor is

$$\rho = (\rho_0 + \rho_1)e^{-g/2} \tag{6}$$

with

$$g = \left(\frac{2\pi \cdot \Delta \cdot (\cos\theta_1 + \cos\theta_2)}{\lambda}\right)^2 \tag{7}$$

where ρ_0 is the scattering coefficient corresponding to the specular reflection, and ρ_1 is the corresponding one due to the diffusely scattered field; Δ is the standard deviation of the surface roughness, θ_1 and θ_2 are the angles of incidence and reflection. When $g = 0$ (smooth surface), $g \ll 1$ (slightly rough), $g \geq 1$ (moderately rough) and $g \gg 1$ (very rough), the scattering patterns are shown in Fig. 3(a)–(d) [19]. From the scattering patterns, we know that when the surface is rough enough, the reflection angles can be different from the incident angles, and the receive antennas can get the signals from different positions. Therefore, this effect can lead to many diffusely scattered multi-path components [17]–[19], and rough surfaces have more reflection spots than smooth surfaces. As shown in Fig. 4(a) and (b), when the transmit antenna is an omnidirectional antenna, only one path exists if the surface is smooth while multiple paths exist if the surface is rough. This means that when the transmit antenna is highly directional, it can only radiate signals to one direction (specular reflection direction) if the surface is smooth; on the other hand, if the surface is rough enough, the transmit antenna can send signals in different directions and the receive antenna can still receive them, as the non-specular reflection paths are strong enough to provide stable links.

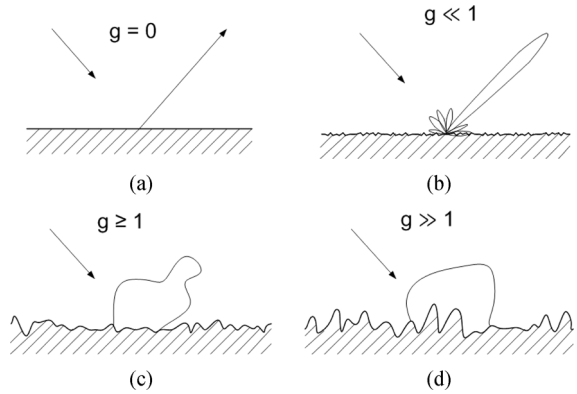

Fig. 3. Transition from specular reflection to diffuse scattering. The surfaces are: (a) smooth; (b) slightly rough; (c) moderately rough; and (d) very rough. Data from [19].

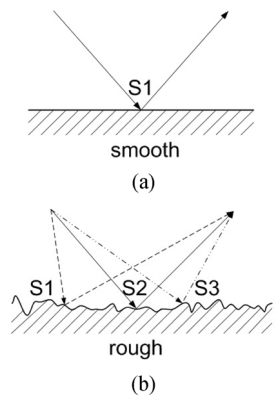

Fig. 4. (a) Single spot reflection from a smooth surface and (b) multiple spot reflection from a rough surface.

IV. Reconfigurable MIMO System

A. Model of the MIMO System

The aforementioned effect makes the THz MIMO model different from that in the GHz band. In this chapter, we consider a systems with M transmit antennas and N receive antennas, and the channel can be represented as an $M \times N$ matrix $\mathbf{H}$. The time invariant channel is described as

$$\mathbf{y} = \mathbf{H}\mathbf{x} + \mathbf{w} \tag{8}$$

where $\mathbf{x}$ is the transmit signal, $\mathbf{y}$ is the receive signal and $\mathbf{w}$ is the white Gaussian noise. The capacity of the channel is [12]

$$C = \sum_{i=1}^{n_{\min}} \log_2\left(1 + \frac{P_i\lambda_i^2}{N_0}\right) \text{ b/s/Hz} \tag{9}$$

where $n_{\min}$ is the rank of $\mathbf{H}$, P_i is the transmit power, N_0 is the noise power spectral density and $\lambda_1, \lambda_2, \ldots, \lambda_{n_{\min}}$ are the singular values of the channel matrix $\mathbf{H}$. In recent years, much ef-

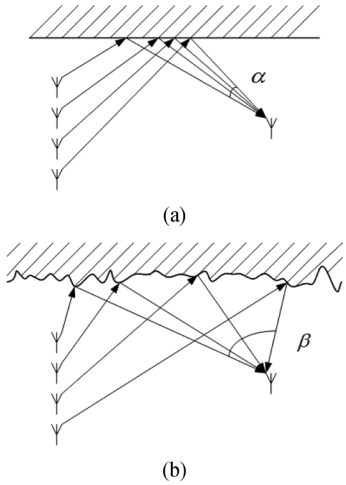

Fig. 5. Angular spreads when the surface is (a) smooth and (b) rough.

fort has been invested to increase this capacity, such as using optimistic power allocation schemes, increasing the rank of $\mathbf{H}$ [12] or using massive MIMO [38]. For most cases, the limited area on the device is the main concern in increasing the rank of $\mathbf{H}$ and implementing enough antennas. For example, $\mathbf{H}$ is ill-conditioned if the antenna separation is too small. Meanwhile, when the separation is large, the number of antennas on the device will be small . Therefore, there is a tradeoff between the number of antennas and the condition of $\mathbf{H}$. For the GHz MIMO, we know from [12] that, the minimum transmit antenna separation normally is $\lambda_c/2$, where λ_c is the wavelength of the signal in free space. If the separation is far less than $\lambda_c/2$, then the signals from two transmit antennas cannot be resolved by the receive antennas, and there is effectively only one degree of freedom. Therefore, it is useless to pack too many antennas in a given amount of space as the angular resolvability does not increase.

However, for the THz MIMO, if all the transmit antennas are highly directional, then the transmit antenna separation can possibly be below $\lambda_c/2$. The reason can be explained as follows. If one directional antenna radiates in a selected direction, because of the rough surfaces, it has high probability that the link is strong enough, as shown in Fig. 4(b). It means that in a certain angle range, the highly directional antennas can choose any radiation directions to establish the link. Therefore, two neighboring antennas can radiate in different directions, and the angular spreads at THz frequencies are larger than those in the GHz range, which means the transmit antenna separation can be smaller than $\lambda_c/2$ in the THz, as shown in Fig. 5. On the other hand, as the atmospheric attenuation is quite strong and the free space loss is high, in order to guarantee a better transmission link, it is also a requirement to use high gain directional antennas in the THz band. Therefore, for THz MIMO systems, not only the graphene-based antenna size is extremely small, but also the antenna separation can be much smaller than the free-space wavelength. This phenomenon can allow the device to accommodate more antennas and increase the channel capacity as a result.

Following the aforementioned analysis, we propose a reconfigurable MIMO antenna design for THz communications based on graphene antennas. The transmitter in our system has an array of antennas and each antenna is an array of nano-patches. The salient features of the design are as follows.

- The transmit antenna separation is smaller than that in GHz MIMO systems. A separation less than $\lambda_c/2$ can make the transmit antenna array smaller and accommodate more antennas on the same area.
- Each antenna in the MIMO system is a highly directional antenna with different radiation directions, and the directions can be configured dynamically. By changing the radiation directions, the transmit antennas can choose the best paths according to the environment.
- The highly directional antenna is made of an array of nano-patches and its radiation pattern is controlled by the states of each graphene patch. The size of graphene-based nano-patch is much smaller than that of a traditional metallic nano-patch, and the states can be easily changed by the electrostatic bias voltage. The patches in the high resistance state are assumed not to introduce interference to the radiation pattern.
- For all the directional antennas, there exists one best radiation direction set that makes the capacity largest. If the channel side information (CSI) is known at the transmitter side, then such best set can be obtained by solving an optimization problem or rolling all the possible sets.

B. Formulation for the Optimal Configuration

For the sake of clarity and briefness, we first use a 2×2 MIMO system as an example. The model setup is shown in Fig. 6. Let h_{ij} denote the channel gain between the ith transmit antenna and the jth receive antenna. Then, we get $[\mathbf{H}]_{i,j} = h_{ij}$ and $h_{ij} = -A_{\text{spread}}(f,d) - A_{\text{abs}} + \rho \cdot \gamma$, where γ is the Fresnel reflection coefficient for a smooth surface. For fixed positions of transmit and receive antennas, h_{ij} is controlled by the incident angle θ_{Ii}. Once the radiation direction is determined, the path length d, the reflection spot, the roughness factor ρ and the reflection angle θ_{Oij} are all obtained. Therefore, for each direction set $[\theta_{I1}, \theta_{I2}]$, there is one unique channel matrix $\mathbf{H}$. The direction set can influence the spectral efficiency in two ways: on one hand, in order to get the lowest path loss, all transmit antennas need to radiate to the same "optimistic" direction which will certainly increase the received signal power; on the other hand, receive antennas cannot distinguish signals from similar directions, thus the degrees of freedom decrease if the directions of the transmit antennas are the same. Thus there is a tradeoff between the received power and the degrees of freedom. Besides, in our example, if the positions of the transmit and receive antennas are known, then the best direction set can also be obtained by solving the following optimization problem:

$$\begin{aligned}
\underset{P_i,\theta_{Ii}}{\text{maximize}} \quad & C = \sum_{i=1}^{n_{\min}} \log_2\left(1 + \frac{P_i \lambda_i^2}{N_0}\right) \ \frac{\frac{\text{b}}{\text{s}}}{\text{Hz}}, \\
\text{subject to} \quad & \sum_{i}^{n_{\min}} P_i \le P \\
& \frac{s_i}{\cos\theta_{Ii}} + \frac{s_{ij}}{\cos\theta_O ij} = d_{ij}, \\
& s_i \tan\theta_{Ii} + s_{ij}\tan\theta_{Oij} = l_{ij}, \\
& h_{ij} = -A_{\text{spread}}(f, d_{ij}) - A_{abs} + \rho
\end{aligned} \tag{10}$$

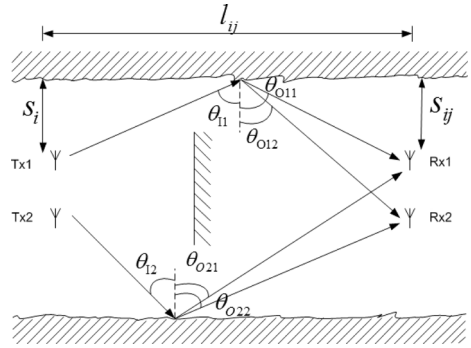

Fig. 6. A MIMO model based on nano-patch antenna array. s_i is the distance between the ith transmit antenna and its reflecting object, s_{ij} is the distance between the jth receive antenna and the ith transmit antenna's reflecting object, and l_{ij} is the horizontal distance between the ith transmit antenna and the jth receive antenna.

where P is the total transmit power, s_i, s_{ij}, l_{ij} are constants shown in Fig. 6, and d_{ij} is the path length between the ith transmit antenna and the jth receive antenna.

When the channel condition is known at both transmitter and receiver sides, the main difficulty in realizing our model is solving the aforementioned optimization problem. Consider the limited computing ability and battery power, it is not possible or necessary to get the optimal solutions using mobile devices. In this situation, we can use a sub-optimal scheme instead of the optimal one. Suppose the radiation direction set is denoted as $\mathbf{D} = [\theta_{I1}, \ldots, \theta_{Ii}, \ldots, \theta_{IN}]$. First of all, we design a group of sets $\mathbf{D}$ in which two identical directions are avoided. In theory, the more the two directions separate from each other, the more independent they are. If the transmit antennas can obtain the feedback from the receive antennas, then an optimal direction set can be achieved by polling all the possible candidate sets. For example, the first antenna radiates to $\pm 15^\circ$ and $\pm 30^\circ$ (the line of sight is 0°) and gets 4 feedbacks from each receive antenna. In the same way, the second antenna can also obtain four feedbacks. Eliminating some unqualified direction sets, only a few direction sets are possible to get the best $\mathbf{H}$. Here the best means the one with the largest rank and eigenvalues. As the environments change quite slowly for indoor communications due to slowly moving objects, we only need to feedback once in a long time period, thus the whole overload is bearable. Finally, we fix the radiation directions and determine the power allocation scheme using the water-filling algorithm. In this algorithm, the direction and the power are not jointly optimized but treated as two independent factors.

Now we consider the scenarios with larger system scales. When the scale is larger than 2×2, such as 4×4 or 8×8, the process is the same as that of 2×2, but with more complex models and workload. When it comes to the massive MIMO range, graphene-based directional antennas are also more suitable than traditional omnidirectional metallic antennas. For example, our antennas can be applied to the dynamic massive MIMO shown in [22]. As we know, the dimension of the antenna array is one of the main obstacles to implementing massive MIMO. By using highly directional graphene antennas, the antenna size and separation are smaller, and the dimensions of the antenna array can be tremendously reduced. Besides, as all the antennas in the array can freely change their directions, the channel state is more random if the antennas randomly choose their directions. Therefore, the assumption that "the fast fading coefficients are assumed to be zero-mean and unit-variance" in [38], [39] is more reasonable, and the final results could be better. When using a zero forcing (ZF) detector, the channel capacity for massive MIMO with M receive antennas is [39]

$$C = \log_2(1 + p_u(M - K)\beta_k) \text{ b/s/Hz} \tag{11}$$

where K is the number of transmit antennas, p_u is the transmit power and β_k denotes the large scale fading factor. For other kinds of detectors, we refer readers to [39] for detailed formulas. Regardless of the detectors, the capacity is highly positively correlated to the number of antennas M. Therefore, graphene-based directional antennas can also promote the capacity of massive MIMO by accommodating more antennas in a given area. The exact performance enhancement would be studied in future work.

V. Results

A. Channel Behavior Analysis

In order to get the capacity of the MIMO system, the path loss in the THz band should be studied first. In our simulations, we set the working frequency as 1 THz which is one of the transmission windows[36] and also results in the corresponding size of the nano-antennas being proper for fabrication. We explore the path loss between the first transmit antenna and the first receive antenna, as shown in Fig. 6. Based on the aforementioned channel model, we know that the path loss is a function of radiation direction and distance. For indoor environments with objects and moving people, we can assume there is no line-of-sight between the transmit and receive antennas [17]. Besides, we can ignore the multi-bounce reflected rays as they are much weaker than single-bounce reflected ray. Therefore, the connections between the transmit and receive antennas are rays with one single-bounce reflection. As discussed in Section III, the path loss in our scenario is contributed by spreading loss, molecular absorption loss and reflection loss. The spreading loss and molecular loss are determined by the transmission distance d while the reflection loss is controlled by the radiation direction. Comparing the wavelength of the signal (300 nm at 1 THz) with the variations of different surfaces (88 nm for plaster and 90 nm for wallpaper [17]), g is on the order of unity and thus the surfaces can be considered as moderately rough.

We first fix the positions of all antennas and reflection objects. The parameters in Fig. 6 are set as follows: $s_1 = 1$ m, $s_{11} = 1$ m and $l_{11} = 2$ m. By increasing the incident angle from 30° to 60°, the spreading loss and the molecular loss vary due to the change of the transmission distance, as shown in Fig. 7(a). The minimum spreading loss is achieved when the incident angle is 45°, as the specular reflection has the shortest transmission distance. However, the other incident angles only slightly increase the spreading loss. The loss due to the roughness factor is obtained using (6), as shown in Fig. 7(b). Interestingly, in this case, the minimum loss is achieved when the incident angle is around 54°, rather than 45°. This means the specular reflection path is not always the best path when the surface is rough enough. Therefore, the total path loss shown in Fig. 7(c) is the combination of the lines in Fig. 7(a) and (b). From Fig. 7(c), we can

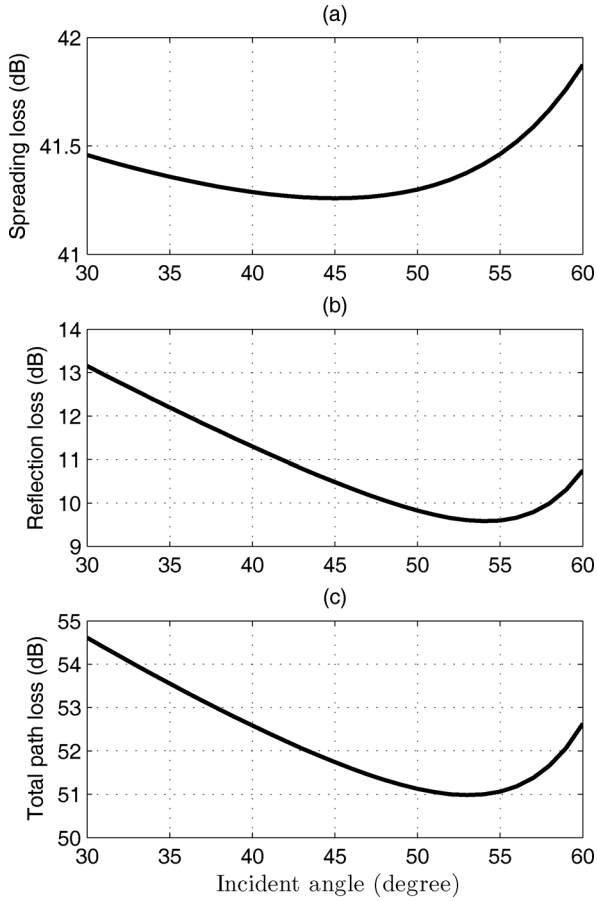

Fig. 7. Path loss between the 1st transmit antenna and the 1st receive antenna with different incident angles.

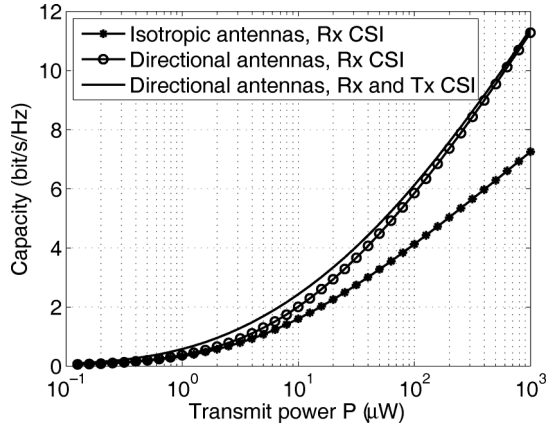

Fig. 8. Capacity of MIMO systems with a size of 2×2. The noise power is 0.01 nW.

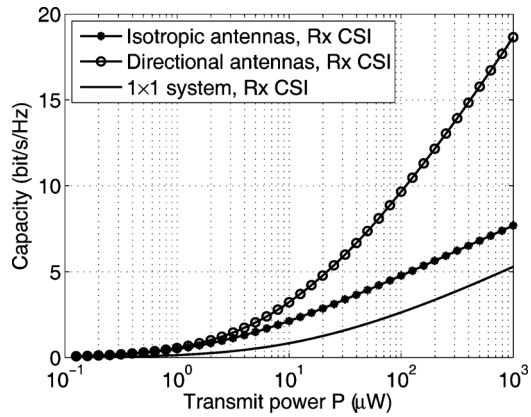

Fig. 9. Capacity of MIMO systems with a size of 4×4. The noise power is 0.01 nW.

get the conclusion that the best path between the transmit and receive antennas is near the specular reflection path, yet other paths are also strong enough to provide stable connections.

B. Channel Capacity Analysis

The channel capacity for 2×2 MIMO with different transmit power is shown in Fig. 8. The parameter setup is the same as that in Fig. 7 and with $s_2 = 1$ m, $s_{12} = 1.5$ m, $s_{21} = 1$ m, $s_{22} = 0.5$ m, and $l_{ij} = 2$ m, $i, j \in \{1, 2\}$. The separation of the two transmit antennas is 0.1 mm (one third of the wavelength) while the separation of the two receivers is 0.5 m (usually the separation of different receivers is on the order of meters). In this simulation, the spectral efficiency is determined by the radiation directions, the transmit power and the noise power. The dotted line (isotropic antennas, Rx CSI) shows the spectral efficiency of the traditional MIMO system model with omnidirectional metallic antennas and smooth surface. The links between the transmitters and the receivers are all specular reflected rays. As a comparison, the circle line (directed antennas, Rx CSI) shows the spectral efficiency of the MIMO system with directional antennas. The spectral efficiency is higher than the dotted line which is more obvious when the transmit power is large. The reason is that under our assumptions, the system can fully use all of the degrees of freedom even if the antenna separation is small and the scattered rays are limited. Furthermore, the solid line (directed antennas, Rx and Tx CSI) is the spectral efficiency of the system with the best power allocation scheme. In this example, we assume the CSI is known by the transmit antennas and the water-filling power allocation scheme is used. The advantage of the water-filling scheme is more obvious in the low transmit power range. When the transmit power is high, the difference between the schemes with and without power allocation is negligible.

Fig. 9 shows the channel capacity for a 4×4 MIMO system. The distance between the transmitter and the receiver is 2 m. In this case, each of the antennas radiates in different directions, making the paths independent to each other. As in Fig. 8, the dotted line is the capacity (isotropic antennas, Rx CSI) of a traditional MIMO system with omnidirectional antennas. The spectral efficiency is less than 4 times that of 1×1 system (the solid line)[12, p. 399]. This is because there are not enough scattered rays between the transmitters and the receivers. As a result, the transmit antennas with limited separation cannot be distinguished by the receive antennas, and the channel matrix $\mathbf{H}$ is ill-conditioned. Compared with the dotted line in Fig. 8, we can see that doubling antennas does not double the channel capacity, but only increases it by 1 bit/s/Hz. It indicates that more antennas only provide diversity instead of degrees of freedom if they are too close to each other. The circle line is the capacity of our proposed system with 4 antennas. The capacity is

almost 4 times that of 1×1 system (the solid line). This means the system can benefit from all the degrees of freedom. The capacity is a little lower than that of the traditional MIMO systems with full scattering [12, Fig. 8.2] as the non-specular reflections can introduce some loss. For other different antenna positions, systems dimensions, and propagation environments, the optimal allocated power and the best antenna configurations can be obtained by solving (10).

VI. Conclusion

A new MIMO antenna system with graphene-based antennas for THz communications has been proposed. The results have shown that the proposed MIMO system has a higher spectral efficiency than the traditional MIMO systems with omnidirectional metallic antennas. By using the water-filling power allocation scheme, the spectral efficiency increases to an even higher level. The main difficulty in our model is solving the optimization problem considering the limited computing ability of the devices.Therefore, a sub-optimal solution has been presented as a supplement to the optimal one, providing a tradeoff between complexity and accuracy.

Acknowledgment

The authors would like to express their appreciation to Dr. T. Lu of the University of Victoria, Victoria, BC, Canada, for useful discussions on graphene properties and suggestions on Yagi–Uda antennas.

References

[1] K. S. Novoselov, A. K. Geim, S. V. Morozov, D. Jiang, Y. Zhang, S. V. Dubonos, I. V. Grigorieva, and A. A. Firsov, "Electric field effect in atomically thin carbon films," *Science*, vol. 306, pp. 666–669, Oct. 2004.

[2] Y. M. Lin, C. Dimitrakopoulos, K. A. Jenkins, D. B. Farmer, H. Y. Chiu, A. Grill, and P. Avouris, "100-GHz transistors from wafer-scale epitaxial graphene," *Sci.*, vol. 327, pp. 662–662, Feb. 2010.

[3] R. Murali, K. Brenner, Y. Yang, T. Beck, and J. D. Meindl, "Resistivity of graphene nanoribbon interconnects," *IEEE Electon Device Lett.*, vol. 30, no. 6, pp. 611–613, Jun. 2009.

[4] K. I. Bolotin, K. J. Sikes, Z. Jiang, M. Klima, G. Fudenberg, J. Hone, P. Kim, and H. L. Stormer, "Ultrahigh electron mobility in suspended graphene," *Solid State Commun.*, vol. 146, pp. 351–355, Jun. 2008.

[5] X. Du, I. Skachko, A. Barker, and E. Y. Andrei, "Approaching ballistic transport in suspended graphene," *Nat. Nanotechnol.*, vol. 3, pp. 491–495, Aug. 2009.

[6] M. Dragoman, A. A. Muller, D. Dragoman, F. Coccetti, and R. Plana, "Terahertz antenna based on graphene," *J. Appl. Phys.*, vol. 107, p. 104313, 2010.

[7] I. Llatser, C. Kremers, D. N. Chigrin, J. M. Jornet, M. C. Lemme, A. C. Aparicio, and E. Alarcon, "Characterization of graphene-based nano-antennas in the terahertz band," in *Proc. 6th EuCAP*, Mar. 2012, pp. 194–198.

[8] J. M. Jornet and I. F. Akyildiz, "Graphene-based nano-antennas for electromagnetic nanocommunications in the terahertz band," in *Proc. 4th EuCAP*, Apr. 2010, pp. 1–5.

[9] I. Llatser, C. Kremers, A. C. Aparicio, J. M. Jornet, E. Alarcon, and D. N. Chigrin, "Graphene-based nano-patch antenna for terahertz radiation," *Photon. Nanostruct: Fundam. Appl.*, vol. 4, pp. 353–358, 2012.

[10] M. Tamagnone, J. S. Gomez-Diaz, J. R. Mosig, and J. Perruisseau-Carrier, "Reconfigurable terahertz plasmonic antenna concept using a graphene stack," *Appl. Phys. Lett.*, p. 214102, 2012.

[11] Y. Huang, L. Wu, M. Tang, and J. Mao, "Design of a beam reconfigurable THz antenna with graphene-based switchable high-impedance surface," *IEEE Trans. Nanotechnol.*, vol. 11, no. 4, pp. 836–842, Jul. 2012.

[12] D. Tse and P. Viswanath, *Fundamentals of Wireless Communication*. Cambridge, U.K.: Cambridge Univ. Press, 2005.

[13] D. Piazza and K. R. Dandekar, "Reconfigurable antenna solution for MIMO-OFDM systems," *Electron. Lett.*, vol. 42, pp. 446–447, Apr. 2006.

[14] J. D. Boerman and J. T. Bernhard, "Performance study of pattern reconfigurable antennas in MIMO communication systems," *IEEE Trans. Antennas Propag.*, vol. 56, no. 1, pp. 231–236, Jan. 2008.

[15] J. M. Jornet and I. F. Akyildiz, "Channel modeling and capacity analysis for electromagnetic wireless nanonetworks in the terahertz band," *IEEE Trans. Wireless Commun.*, vol. 10, no. 10, pp. 3211–3221, Oct. 2011.

[16] R. Piesiewicz, M. Jacob, M. Koch, J. Schoebel, and T. Kurner, "Performance analysis of future multigigabit wireless communication systems at THz frequencies with highly directive antennas in realistic indoor environments," *IEEE J. Sel. Topics in Quantum Electron.*, vol. 14, no. 2, pp. 421–430, Mar./Apr. 2008.

[17] C. Jansen, S. Priebe, C. Moller, M. Jacob, H. Dierke, M. Koch, and T. Kurner, "Diffuse scattering from rough surfaces in THz communication channels," *IEEE Trans. THz Sci. Technol.*, vol. 1, no. 2, pp. 462–472, Nov. 2011.

[18] R. Piesiewicz, C. Jansen, D. Mittleman, T. K. Ostmann, M. Koch, and T. Kurner, "Scattering analysis for the modeling of THz communication systems," *IEEE Trans. Antennas Propag.*, vol. 55, no. 11, pp. 3002–3009, Nov. 2007.

[19] P. Beckmann and A. Spizzichino, *The Scattering of Electromagnetic Waves from Rough Surfaces*. New York, NY, USA: Macmillan, 1963.

[20] I. S. Gregory, C. Baker, W. R. Tribe, I. V. Bradley, M. J. Evans, E. H. Linfield, A. G. Davies, and M. Missous, "Optimization of photomixers and antennas for continuous-wave terahertz emission," *IEEE J. Quantum Electron.*, vol. 41, no. 5, pp. 717–728, May 2005.

[21] G. Georgiou, H. K. Tyagi, P. Mulder, G. J. Bauhuis, J. J. Schermer, and J. G. Rivas, "Photo-generated THz antennas," *Sci. Rep.*, p. 3584, Jan. 2014.

[22] I. F. Akyildiz, J. M. Jornet, and C. Han, "Terahertz band: Next frontier for wireless communications," *Phycical Commun.*, vol. 12, pp. 16–32, Sep. 2014.

[23] I. F. Akyildiz, F. Brunetti, and C. Blazquez, "Nanonetworks: A new communication paradigm," *Comput. Netw.*, vol. 52, pp. 2260–2279, Apr. 2008.

[24] J. S. Gomez-Diaz, M. Esquius-Morote, and J. Perruisseau-Carrier, "Plane wave excitation-detection of non-resonant plasmons along finite-width graphene strips," *Opt. Express*, vol. 21, p. 24856, Oct. 2013.

[25] M. Esquius-Morote, J. S. Gomez-Diaz, and J. Perruisseau-Carrier, "Sinusoidally modulated graphene leaky-wave antenna for electronic beamscanning at THz," *IEEE Trans. THz Sci. Technol.*, vol. 4, no. 1, pp. 116–122, Jan. 2014.

[26] D. Correas-Serrano, J. S. Gomez-Diaz, and A. Alvarez-Melcon, "On the influence of spatial dispersion on the performance of graphene-based plasmonic devices," *IEEE Antennas Wireless Propag. Lett.*, vol. 13, pp. 345–348, Feb. 2014.

[27] G. Lovat, G. W. Hanson, R. Araneo, and P. Burghignoli, "Semiclassical spatially dispersive intraband conductivity tensor and quantum capacitance of graphene," *Phys. Rev. B*, vol. 87, p. 115429, 2013.

[28] V. P. Gusynin, S. G. Sharapov, and J. P. Carbotte, "Magneto-optical conductivity in graphene," *J. Phys.: Cond. Matter*, vol. 19, p. 026222, 2007.

[29] G. W. Hanson, "Dyadic green's function and guided surface waves for a surface conductivity model of graphene," *J. Appl. Phys.*, vol. 103, p. 064302, 2008.

[30] A. Y. Nikitin, F. Guinea, F. J. Garcła-Vidal, and L. Martłn-Moreno, "Edge and waveguide terahertz surface plasmon modes in graphene microribbons," *Phys. Rev. B*, vol. 84, p. 161407, 2011.

[31] K. S. Kim, Y. Zhao, H. Jang, S. Y. Lee, J. M. Kim, K. S. Kin, J. H. Ahn, P. Kim, J. Y. Choi, and B. H. Hong, "Large-scale pattern growth of graphene films for stretchable transparent electrodes," *Nature*, vol. 457, pp. 706–710, Feb. 2009.

[32] P. Chen and A. Alu, "A terahertz photomixer based on plasmonic nanoantennas coupled to a graphene emitter," *Nanotechnol.*, vol. 24, p. 455202, 2013.

[33] T. Otsuji, T. Watanabe, S. A. B. Tombet, A. Satou, W. M. Knap, V. V. Popov, M. Ryzhii, and V. Ryzhii, "Emission and detection of teraherz radiation using two-dimensional electrons in III-V semiconductors and graphene," *IEEE Trans. THz Sci. Technol.*, vol. 3, no. 1, pp. 63–71, Jan. 2013.

[34] J. M. Jornet and I. F. Akyildiz, "Graphene-based plasmonic nano-transceiver for terahertz band communication," in *Proc. 8th EuCAP*, Apr. 2014, pp. 684–688.
[35] S. Zhang, G. H. Huff, J. Feng, and J. T. Bernhard, "A pattern refonfigurable microstrip parasitic array," *IEEE Trans. Antennas Propag.*, vol. 52, no. 10, pp. 2773–2776, Oct. 2004.
[36] K. Huang and Z. Wang, "Terahertz terabit wireless communication," *IEEE Microw. Mag.*, pp. 108–116, Jun. 2011.
[37] H. Song and T. Nagatsuma, "Present and future of terahertz communications," *IEEE Trans. THtz Sci. Technol.*, vol. 1, no. 1, pp. 256–263, Sep. 2011.
[38] T. L. Marzetta, "Noncooperative cellular wireless with unlimited numbers of base station antennas," *IEEE Trans. Wireless Commun.*, vol. 9, no. 11, pp. 3591–3600, Nov. 2010.
[39] H. Q. Ngo, E. G. Larsson, and T. L. Marzetta, "Energy and spectral efficiency of very large multiuser MIMO systems," *IEEE Trans. Commun.*, vol. 61, no. 4, pp. 1436–1449, Apr. 2013.

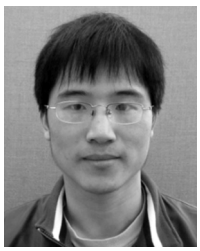

Zheng Xu received the B.Sc. degree in telecommunication from Jilin University, China in 2008, the M.Sc. degree in telecommunication from Beijing University of Posts and Telecommunications, Beijing, China, in 2011, and is currently working towards the Ph. D degree at the Department of Electrical and Computer Engineering, University of Victoria, Victoria, BC, Canada.

His research interests include electromagnetic nanonetworks, graphene-based wireless communication, and terahertz band communication.

Xiaodai Dong (S'97–M'00–SM'09) received the B.Sc. degree in information and control engineering from Xi'an Jiaotong University, China, in 1992, the M.Sc. degree in electrical engineering from National University of Singapore in 1995, and the Ph.D. degree in electrical and computer engineering from Queen's University, Kingston, ON, Canada, in 2000.

Since January 2005, she has been with the University of Victoria, Victoria, Canada, where she is now a Professor and Canada Research Chair (Tier II) at the Department of Electrical and Computer Engineering. Between 2002 and 2004, she was an Assistant Professor at the Department of Electrical and Computer Engineering, University of Alberta, Edmonton, AB, Canada. From 1999 to 2002, she was with Nortel Networks, Ottawa, ON, Canada and worked on the base transceiver design of the third-generation (3G) mobile communication systems. Her research interests include communication theory, radio propagation, ultra-wideband radio, machine to machine communications, wireless security, smart grid, nano communications, and signal processing for communication applications.

Dr. Dong is an Editor for IEEE TRANSACTIONS ON WIRELESS COMMUNICATIONS, IEEE TRANSACTIONS ON VEHICULAR TECHNOLOGY, and the *Journal of Communications and Networks*.

Jens Bornemann (M'87–SM'90–F'02) received the Dipl.-Ing. and the Dr.-Ing. degrees, both in electrical engineering, from the University of Bremen, Germany, in 1980 and 1984, respectively.

From 1984 to 1985, he was a consulting engineer. In 1985, he joined the University of Bremen, Germany, as an Assistant Professor. Since April 1988, he has been with the Department of Electrical and Computer Engineering, University of Victoria, Victoria, BC, Canada, where he became a Professor in 1992. From 1992 to 1995, he was a Fellow of the British Columbia Advanced Systems Institute. In 1996, he was a Visiting Scientist at Spar Aerospace Ltd. (now MDA Space), Ste-Anne-de-Bellevue, QC, Canada, and a Visiting Professor at the Microwave Department, University of Ulm, Ulm, Germany. In 2003, he was a Visiting Professor at the Laboratory for Electromagnetic Fields and Microwave Electronics, ETH Zurich, Switzerland. From 1997 to 2002, he was a co-director of the Center for Advanced Materials and Related Technology (CAMTEC), University of Victoria. He has coauthored *Waveguide Components for Antenna Feed Systems—Theory and Design* (Artech House, 1993) and has authored/coauthored more than 250 technical papers. His research activities include RF/wireless/microwave/millimeter-wave components and systems design, and field-theory-based modeling of integrated circuits, feed networks, ultra-wideband technology and antennas.

Dr. Bornemann is a Registered Professional Engineer in the Province of British Columbia, Canada. He is a Fellow of the Canadian Academy of Engineering (CAE), and serves on the editorial advisory board of the *International Journal of Numerical Modelling*. From 1999 to 2002, he served as an Associate Editor of the IEEE TRANSACTIONS ON MICROWAVE THEORY AND TECHNIQUES in the area of Microwave Modeling and CAD. From 2006 to 2008, he was an Associate Editor of the *International Journal of Electronics and Communications*. From 1999 to 2009, he served on the Technical Program Committee of the *IEEE MTT-S International Microwave Symposium*.